AIAA 94-2205

VALIDATION OF AN ANALYTICAL MODEL FOR AN UNSTEADY PLANAR JET WITH SELF-SUSTAINED OSCILLATIONS

F. Herr and C. Camci

Department of Aerospace Engineering
The Pennsylvania State University
University Park, PA 16801

25th AIAA Fluid Dynamics Conference

June 20-23, 1994 / Colorado Springs, CO

VALIDATION OF AN ANALYTICAL MODEL FOR AN UNSTEADY PLANAR JET WITH SELF-SUSTAINED OSCILLATIONS

Frank Herr† and Cengiz Camci‡
Department of Aerospace Engineering
Turbomachinery Heat Transfer Laboratory
The Pennsylvania State University
University Park, Pennsylvania

ABSTRACT

Flow field in an oscillatory plane jet with self-sustained oscillations was studied by using a corrected similarity solution and the an analytical unsteady flow model was validated via hot wire measurements. A decomposition approach was used to identify the contribution due to the deterministic flow field oscillations and stochastic turbulent fluctuations. To realize this decomposition, an accurate, efficient hot wire technique based on a crossed wire sensor was implemented. The governing equations were derived for flows containing deterministic oscillations of fixed frequency. Both experiments and analysis prove that oscillation stresses contribute to the transport process and that the double velocity correlations obtained from oscillation fluctuations and turbulent fluctuations are negligible compared to Reynolds and oscillation stresses. This feature simplifies the equations and the analysis significantly. The present corrected similarity solution predicts planar oscillatory jet flow quite well. The instantaneous deterministic part of the flow field can be calculated with reasonable accuracy. Mean velocity, oscillation stresses, oscillation kinetic energy predictions from the new analytical model developed in this study are in very close agreement with the measured data.

NOMENCLATURE

b :	Coefficients of Fourier integral, jet width
d :	Jet throat width
E :	Hot wire voltage
f :	Jet oscillatory frequency
K :	Kinematic momentum $= \int_{-\infty}^{\infty} U^2 dy$
M, N :	Numbers of calibration velocity and angle settings
p :	Turbulent pressure fluctuation
P :	Mean pressure
q^2 :	Turbulent kinetic energy $= u^2 + v^2 + w^2$
q^{*2}	Oscillatory kinetic energy $= u^{*2} + v^{*2} + w^{*2}$
Re	Reynolds number $= U_0 d/\nu$
t :	time
T :	Diffusion, period of oscillation
u, v, w :	Velocity fluctuations, also u_1, u_2, u_3
U, V :	Mean velocity
x :	Axial distance from the jet exit
y :	Lateral distance from the jet centerline
α :	Jet oscillation angle
β :	Non-dimensionalization factor $= x/{U_m}^3$
ϵ :	Dissipation rate
η :	Similarity variable $= y/x$
κ_1 :	free jet constant
ρ :	Density
σ :	Empirical jet constant
ν :	Kinematic viscosity, turbulent diffusivity
θ :	Temperature fluctuation, calibration yaw angle
Θ :	Mean temperature
γ :	Thermal diffusivity, hot wire setting angle

Subscripts, superscripts and symbols

$<>$:	Time averaged mean value
$\overline{\overline{<>}}$:	Ensemble averaged mean value
$*$:	Deterministic (ensemble averaged) mean value
$**$:	Transformed hot wire quantity
	Intermediate variable in calibration
$'$:	Relative coordinates
$\tilde{}$:	Instantaneous quantity
i, j, k :	Coordinates
0:	Condition when time $t = 0$
m :	Mean value at jet centerline
t :	turbulent

† Graduate Research Assistant, Student Member AIAA

‡ Associate Professor of Aerospace Engineering, Member AIAA

Introduction

Jet flows are used in a wide spectrum of engineering applications. The steady turbulent jet is a well-documented flow and has many practical uses such as ejectors, burners, coolant jets, etc.. The unsteady jet has also been a useful tool in engineering applications such as pulsating combustion and thrust augmentation devices using ejectors, mixers, etc.. The main objective of this study is to investigate the flow field and transport mechanisms in a plane jet flow with self-sustained oscillations using a recently developed analytical model. The model development is also supported by hot wire measurements.

There are many ways to create oscillatory jets. Acoustic excitation can increase the spreading rate of a jet under certain conditions (Crow and Champagne, 1971). Further increases in the spreading rate can be obtained by multifrequency plane-wave excitation (Ho and Huang, 1982). The use of an acoustic driver is not practical due to its complexities. The limitations of acoustic excited oscillation can be overcome by a number of mechanical means such as rotating valves (Binder and Favre-Marinet, 1973), oscillating vanes (Rockwell, 1972), and self-excitation using counterflow (Strykowski, 1992). However, for practical applications, the excitation techniques should be simple and effective. Several simple devices have been developed to enhance jet mixing, such as self-exciting whistler nozzle (Hussain and Hasan, 1983), and the screech-excited jet (Glass, 1968). The fluidic oscillatory jet nozzle developed by Viets (1975) is one of the simplest and effective devices to enhance the mixing process. This type of oscillatory jet was extended to supersonic flow by Raman, Hailye and Rice (1993).

The oscillation of the driving flow is an effective way to enhance momentum and heat transfer. Previous computational and experimental studies of oscillatory flows indicated modified mass, momentum and heat transfer. However, the study of mechanism of transport enhancement by flow oscillation, compared to steady problems, is far from satisfactory. Many previous investigations on oscillatory jets were focused on mean velocity and spreading rate measurements. No results have been reported on turbulent flow quantities, energy balance and distribution in this type of flow. It is necessary to carry out a detailed analysis based on momentum, thermal and kinetic energy transport equations. More comprehensive measurements of mean flow, periodic (deterministic) and turbulent flow are needed in support of the analysis. The present paper examines, analytically and experimentally, the problems associated with the unsteady flow with self-sustained oscillations.

It is a known fact that the jet spreading and volumetric entrainment increase in oscillatory jet flows. However, the fundamental structure of the flow field does not change when compared to stationary jet. The experimental observations of the present study show that the velocity profiles are self-similar; the spreading rate is linear with downstream distance (Herr and Camci, 1994). The oscillatory jet results are consistent with that of the stationary jet from self-similarity point of view, except for the proportionality constants. All of the previous unsteady jet studies show that the steady jet characteristics are recovered once a certain downstream location is reached. Previous experimental observations suggest that there might be a similarity solution for oscillatory flow. The establishment of a similarity solution for an oscillatory flow may significantly simplify the studies dealing with the understanding of unsteady flows and unsteady transport mechanisms.

A corrected similarity solution approach to solve the unsteady jet is proposed and validated by the experimental data. Measurements of instantaneous velocity components in the plane jet are made using a crossed hot wire. Mean velocity, turbulence and oscillation stresses, as well as kinetic energy and its components are obtained. Mean velocity, oscillation stresses and oscillation kinetic energy predictions from the corrected similarity solution are in very close agreement with the measured data.

Analytical considerations

Mass, momentum and thermal energy conservations

The instantaneous velocity and temperature can be decomposed into three parts (Hussain and Reynolds, 1970), time averaged quantity (U_i, Θ), ensemble averaged oscillations $(U_i{}^*, \theta^*)$ and turbulent fluctuations (u_i, θ) as shown in figure 1.

$$\tilde{u}_i = U_i + u_i{}^* + u_i, \quad \tilde{\theta} = \Theta + \theta^* + \theta. \tag{1}$$

In addition, one can show that the mean value of turbulent quantities are zero

$$< u_i >= 0, \quad < \theta >= 0. \tag{2}$$

The time averaged deterministic fluctuations of velocity components and temperature are also zero by definition as,

$$< u_i{}^* >= 0, \quad < \theta^* >= 0. \tag{3}$$

In oscillatory flows, the continuity equation can be decomposed as,

$$\frac{\partial U_i}{\partial x_i} + \frac{\partial u_i{}^*}{\partial x_i} + \frac{\partial u_i}{\partial x_i} = 0. \quad (4)$$

Taking time and ensemble average of equation (4) respectively, it can be shown that U_i, $u_i{}^*$ and u_i are all divergence free. Details of this development are given in Herr and Camci (1994).

By decomposing and taking time average of instantaneous momentum equation, one obtains

$$\frac{\partial U_i U_j}{\partial x_j} = -\frac{1}{\rho}\frac{\partial P}{\partial x_i} + \frac{\partial}{\partial x_j}(\nu\frac{\partial u_i}{\partial x_j} - < u_i{}^* u_j{}^* > - < u_i{}^* u_j > - < u_i u_j{}^* > - < u_i u_j >). \quad (5)$$

where $\nu(\partial u_i/\partial x_j)$ and $- < u_i u_j >$ are viscous and turbulent Reynolds stresses, respectively. The term $- < u_i{}^* u_j{}^* >$ is important in oscillatory flow and is termed as oscillation stress in this study. It can be proven that the other two terms $- < u_i{}^* u_j >$ and $- < u_i u_j{}^* >$ are negligible. Double velocity correlations of deterministic oscillations and turbulent fluctuations can be shown as negligible for a constant oscillation frequency f_0 by using Fourier analysis, Herr and Camci (1994). The negligible double velocity correlations obtained from Fourier analysis are also confirmed by hot wire measurements obtained in this study.

Finally, the the time averaged momentum equation for a flow with self-sustained oscillations is as follows.

$$\frac{\partial U_i U_j}{\partial x_j} = -\frac{1}{\rho}\frac{\partial P}{\partial x_i} + \frac{\partial}{\partial x_j}(\nu\frac{\partial u_i}{\partial x_j} - < u_i{}^* u_j{}^* > - < u_i u_j >). \quad (6)$$

The instantaneous thermal energy equation may also be written, with the help of decomposition equation (1) , as

$$\frac{\partial (U_j \Theta)}{\partial x_j} = \frac{\partial}{\partial x_j}(\gamma\frac{\partial \Theta}{x_j} - < u_j{}^* \theta^* > - < u_j \theta^* > - < u_j{}^* \theta > - < u_j \theta >). \quad (7)$$

Similar to the developments leading to equation (6), the terms $< u_j \theta^* >$ and $< u_j{}^* \theta >$ can also be shown to be negligible small by Fourier analysis. Thus the time averaged thermal energy equation for oscillatory flow is

$$\frac{\partial (U_j \Theta)}{\partial x_j} = \frac{\partial}{\partial x_j}(\gamma\frac{\partial \Theta}{x_j} - < u_j{}^* \theta^* > - < u_j \theta >), \quad (8)$$

where $\gamma(\partial\Theta/\partial x_j)$, $- < u_j{}^* \theta^* >$ and $- < u_j \theta >$ are conduction heat flux, oscillation heat flux and turbulent heat flux, respectively.

Transport equation for turbulent oscillatory stresses

The equation governing the transport of turbulent and oscillatory stresses can be obtained by multiplying the Navier-Stokes equations by u_j and $u_j{}^*$, respectively. For the case of oscillatory flow, the oscillation transport equation governing the double velocity correlations in the deterministic sense can be written as

$$\frac{\partial}{\partial t} < u_i^* u_j^* > + < u_i^* u_k^* > \frac{\partial U_j}{\partial x_k} + < u_j^* u_k^* > \frac{\partial U_i}{\partial x_k} + U_k \frac{\partial < u_i^* u_j^* >}{\partial x_k} + \frac{\partial}{\partial x_k} < u_i^* u_j^* u_k^* > = -\frac{1}{\rho}(\frac{\partial}{\partial x_i} < p^* u_j^* > + \frac{\partial}{\partial x_j} < p^* u_i^* >) + \frac{1}{\rho} < p^* (\frac{\partial u_j^*}{\partial x_i} + \frac{\partial u_i^*}{\partial x_j}) > + \nu \frac{\partial}{\partial x_k}\frac{\partial}{\partial x_k} < u_i^* u_j^* > -2\nu < \frac{\partial u_i^*}{\partial x_k}\frac{\partial u_j^*}{\partial x_k} > . \quad (9)$$

An oscillation kinetic energy $< q^* >$ conservation equation can also be developed from equation (9)

$$-\frac{1}{2}(U\frac{\partial < q^{*2} >}{\partial x} + V\frac{\partial < q^{*2} >}{\partial y}) - (< u^{*2} > \frac{\partial U}{\partial x} + < v^{*2} > \frac{\partial V}{\partial y} + < u^* v^* > (\frac{\partial V}{\partial x} + \frac{\partial U}{\partial y})) - \frac{1}{2}(\frac{\partial < q^{*2} v^* >}{\partial y} + \frac{\partial < q^{*2} u^* >}{\partial x}) - \epsilon^* = 0. \quad (10)$$

The equation (10) shows that the oscillatory jet flow is governed by the equations similar to that of stationary turbulent flow. It is reasonable to assume that the oscillatory jet flow may also have a similarity solution. The equations can be written in terms of a similarity variable η by using

$$\frac{\partial}{\partial x} = -\frac{\eta}{x}\frac{\partial}{\partial \eta}, \frac{\partial}{\partial y} = -\frac{1}{x}\frac{\partial}{\partial \eta}, U_m{}^2 = \frac{k}{x}.$$

Turbulence convection, production terms for a steady jet and the corresponding terms for the oscillatory jet are expressed by using a similarity variable $\eta = y/x$. A more

detailed discussion on the similarity concepts is given in Herr and Camci (1994).

Corrected similarity solution for oscillatory jet

The stationary two-dimensional turbulent jet has been studied by many researchers using similarity concepts (Schlichting (1968) and Tennekes and Lumley (1972)). The stationary similarity solution usually match the experimental data quite well. In this study the focus area is the unsteady oscillatory jet. The fluidic nozzle generating the bi-stable planar jet flow in this study is shown in figure 2. The planar jet is in a fixed frequency unsteady flapping motion with respect to its longitudinal axis. Based on a stationary jet solution, an oscillatory jet flow model has been developed to investigate the flow field including instantaneous oscillation velocity, oscillation stresses and oscillation kinetic energy. The idea of the corrected oscillatory similarity solution is the following. At a given time t, the unsteady oscillatory flow field can be approximately described by the solution of a stationary jet flow obtained from a nozzle attached to a relative reference frame which is oscillating at a prescribed frequency.

The time averaged governing equations of the stationary two-dimensional turbulent jet for incompressible flow are

$$\frac{\partial U}{\partial x}+\frac{\partial V}{\partial y}=0, \tag{11}$$

$$U\frac{\partial U}{\partial x}+V\frac{\partial V}{\partial y}=\nu_t\frac{\partial^2 U}{\partial y^2}. \tag{12}$$

In the momentum equation, the molecular viscous stresses are neglected because of the fact that they are very small compared to the turbulent counterparts in problems involving free turbulent flows. Based on Prandtl's turbulent mixing length theory, the turbulent viscosity is given by

$$\nu_t=\kappa_1 b U_m, \tag{13}$$

where U_m denotes the mean centerline velocity, κ_1 a free jet constant and b the jet width. The similarity solution to equations (12) and (11) is

$$U=\frac{\sqrt{3}}{2}\sqrt{\frac{K\sigma}{x}}(1-\tanh^2(\sigma\eta)), \tag{14}$$

$$V=\frac{\sqrt{3}}{4}\sqrt{\frac{K}{x\sigma}}\{2\sigma\eta\left(1-\tanh^2(\sigma\eta)\right) -\tanh(\sigma\eta)\}, \tag{15}$$

where K is the kinematic momentum defined as $K=\int_{-\infty}^{\infty}U^2dy$. The empirical constant σ which contains κ_1 is 7.67 as suggested by Schlichting (1968). The present oscillatory jet flow model is set up in such a way that the jet nozzle relative frame is numerically oscillated at a given frequency f. The oscillating jet nozzle issues air at an instantaneous angle of $\alpha=2\pi ft+\alpha_0$ as shown in figure 3.

The stationary frame similarity solution described in equations (14) and (15) is borrowed from the classical similarity solution of Schlichting (1968) and used as relative velocity in the coordinate frame attached to the nozzle oscillating around a point located at the throat section, as shown in figure 3. However, what an observer (located in the absolute frame of reference) sees is severely modified by the oscillation of the relative frame. The present model developed in this study is based on the fact the deterministic oscillation motion of the relative frame attached to the nozzle can be added to the steady similarity solution shown in equations (14) and (15) from a kinematic point of view. However, this instantaneous velocity field significantly altered by the deterministic relative frame oscillations is only an initial prediction of the unsteady field in the absolute frame. One expects that the acceleration of the relative frame also influences the overall unsteady flow field observed from the absolute frame. At this stage, the initial solution is not fully compatible with the unsteady Navier-Stokes equations, because the unsteady forces due to the frame oscillation are not taken into account in the initial velocity distributions. A more realistic unsteady flow solution can be obtained from the ensemble averaged Navier-Stokes equations in an iterative manner, starting from the initial prediction of the unsteady field in the absolute frame.

In figure 3, assume that the point P moves on a circle around O', with radius R at a constant angular velocity $2\pi f$. The line OP simulates the jet centerline of the main stream which oscillates with a maximum sweep angle α_M. Line OP may be visulized as a perfectly elastic wire defining the center line of the jet which oscillates with the relative frame $(x'y')$. Obviously, the relation between α and t is

$$\tan\alpha=\frac{R\sin(2\pi ft+\alpha_0)}{\frac{R}{\sin\alpha_M}+R\cos(2\pi ft+\alpha_0)} \tag{16}$$

where α_0 is the initial angle corresponding to $t=0$. The instantaneous velocity in x',y' and x,y system are denoted $U_{x'},_{y'}$, $V_{x'},_{y'}$ and U,V, respectively. The coordinate transformation between the relative orthogonal system x',y' attached to the oscillating nozzle and the absolute

orthogonal system x, y as shown in figure 4 is as follows.

$$x' = x\cos\alpha + y\sin\alpha, \quad (17)$$

$$y' = x\sin\alpha - y\cos\alpha. \quad (18)$$

With these definitions, the classical turbulent similarity solution (equations (14) and (15) for the stationary jet can be written in the relative frame of reference (x', y').

An initial estimate of the instantaneous velocity profile can be developed as the sum of the stationary similarity solution in the relative frame and the induced x and y velocity components due to the relative frame oscillations at a given time t. The initial x and y components of instantaneous deterministic velocity can be estimated as follows.

$$U_{initial} = U_{x'y'}\cos\alpha + V_{x'y'}\sin\alpha - \frac{d\alpha}{dt}\sqrt{x'^2 + y'^2}\sin(\alpha - \tan^{-1}\frac{y'}{x'}), \quad (19)$$

$$V_{initial} = U_{x'y'}\sin\alpha - V_{x'y'}\cos\alpha - \frac{d\alpha}{dt}\sqrt{x'^2 + y'^2}\cos(\alpha - \tan^{-1}\frac{y'}{x'}). \quad (20)$$

As shown in figure 4, the first two terms of the equations (19) and (20) represent the stationary similarity solution contribution to the overall flow field description. The remaining terms can be obtained as the induced x and y velocity components created by the relative frame oscillations.

The solution expressed by equations (19) and (20) must be corrected to satisfy the unsteady Navier-Stokes equations. As observed from the stationary frame (x, y), the instantaneous deterministic velocities U^* and V^* are defined as

$$U^* = U + u^*,$$

$$V^* = V + v^*.$$

The governing equations of deterministic motion for two-dimensional unsteady jet are obtained by taking ensemble average of instantaneous x-momentum equation and continuity equation.

$$\frac{\partial U^*}{\partial t} + U^*\frac{\partial U^*}{\partial x} + V^*\frac{\partial U^*}{\partial y} = \frac{\partial}{\partial y}(-\overline{\overline{< uv >}}), \quad (21)$$

$$\frac{\partial U^*}{\partial x} + \frac{\partial V^*}{\partial x} = 0, \quad (22)$$

where $\overline{\overline{< uv >}}$ denotes the ensemble averaged turbulent stress. This equation controls the dynamics of the deterministic unsteady fluid motions. The influence of the stochastic turbulent fluctuations on U^* is represented by the right hand side of equation (21). The present hot wire measurements as shown in figure 10 show that the time averaged turbulent stress in the current oscillatory jet is approximately equal to the ensemble averaged turbulent stress. For a self-preserving jet, the second momentum equation is negligible based on the order of magnitude analysis. Although a direct solution of momentum and continuity equations could be obtained by numerical schemes and large computer time and memory, in this study, a simple iterative approach is used to find out instantaneous U^* and V^*. The momentum and continuity equations can be rearranged as follows.

$$V^* = -\frac{1}{\frac{\partial U^*}{\partial y}}(\frac{\partial U^*}{\partial t} + U^*\frac{\partial U^*}{\partial x} - \frac{\partial}{\partial y}(-\overline{\overline{< uv >}})), \quad (23)$$

$$U^* = -\int \frac{\partial V^*}{\partial y}dx. \quad (24)$$

An initial estimate of U^* ($U_{initial}$ in equation (19)) and ensemble averaged turbulent stress ($- < \overline{uv} > = < uv >$) from the measured data as shown in figure 10 can be differentiated and substituted into equation (23) in order to obtain a better estimate of V^*. The new value of V^* may then be differentiated and substituted into the continuity equation (24) to generate a more accurate value for U^*. This process is repeated until a predefined convergence is achieved on both U^* and V^*. Details of the numerical procedure is given in Herr (1994).

Experimental setup and procedure

Experimental setup

The operation principle of the present oscillatory jet is based on the fact that a jet exiting into space between two sufficiently near walls is bi-stable, i.e may attach to either wall. In addition, a small pressure disturbance across the jet at its thorat section may cause the jet to detach one wall and attach to the opposite one. A simple fluidic nozzle representation of the oscillatory jet used in this study is shown in figure 2. The air flows through a contraction, past two communication ports, into an expansion section. The output ports are attached to each other via a communication loop. Due to the proximity of the wall at the jet throat, the jet is bi-stable and must attach to one of the walls. The large amount of entrainment of

air will pull the jet stream back to the other wall. Thus in a well designed nozzle, the jet will oscillate between walls. The constant frequency of oscillation is controled by the length and diameter of the communication loop. The comppression and expansion waves in the communication line travel from one port to the other port located at the end of the loop. The frequency is also a function of stagnation pressure entering the system. The improved mixing characteristics of the oscillatory jet are seen in the increased spread angle and in the voids of stagnant gas which are entrained between waves of the oscillation.

A series of nozzles were manufactured. The side walls are made of $1\frac{1}{2}$ inch ($3.8cm$) thick plexiglass. Based on the experience from different test nozzles, two sets of aluminium nozzle with fine spline fitted surface contours were carefully machined by a numerically controlled milling machine.

A regulated laboratory compressed air supply from 70 psi line was fed into the nozzle. The jet emerged from the nozzle having a 5 mm throat width at a mean velocity of 25 m/s (Re=10^4). The longer dimension of the rectangular nozzle cross section was 25.4 mm. To study the oscillation caused by the mechanism described above, the unsteadiness of other means must be minimum. With two communicating ports closed, the velocity at the nozzle throat was maintained constant to an accuracy better than 1%. For steady flow situation, at the exit plane the jet is essentially laminar, having a turbulent intensity of approximately 0.1%.

Measurements were taken with a TSI 1249A-T1.5 miniature 90^0 crossed hot wire probe, a TSI1210-T1.5 general purpose single sensor probe and TSI series 1050 constant temperature anemometers. The single sensor probe was used to measure the jet exit velocity. The wires were mounted on a two-dimensional traverser which spans the entire flow field for a fixed x location.

Calibration Technique

The decomposition of instantaneous velocities into time mean, deterministic mean and turbulent fluctuations requires a probe calibration with high accuracy and resolution. A full velocity yaw angle calibration scheme with a coordinate transformation was used to meet these requirements. The crossed wire probe was calibrated in a calibration jet with velocity ranging from 0.5 to 40 m/s. The calibration domain consists of angular range of $\pm 45^0$ and a velocity range from 0.5 to 25 m/s. At each setting of velocity and yaw angle, the true air speed of the calibration jet was measured by a pitot probe and a pair of voltages (E_1, E_2) was acquired by a computer data acquisition system. The specific calibration scheme was first used by Lueptow et. al (1988) and modified by Panchepakesan and Lumley (1993). A brief outline of this technique is as follows.

1. with 14 by 21 pairs of (E_1, E_2) raw data, a raw calibration look-up table was made as shown in figure 4(a).

2. A stretching transformation was applied to the raw data to convert them from (E_1, E_2) to (U^{**}, θ^{**}). This transformation is based on the fact that the King's law (or polynomial fit) and Cosine law are approximately accurate for each of the single sensor of a crossed wire. The transformation is presented in figures 7 and 8.

3. Cubic spline fits along each N lines are used to find U^{**} and Q each as function of θ^{**}.

4. For 400 points between ${U^{**}}_{min}$ and ${U^{**}}_{max}$, U^{**} and Q are evaluated for each angle γ by using curve fitting given by the previous step.

5. Using the spline fits determined above, the values for γ and Q are calculated at 400 points between ${\theta^{**}}_{min}$ and ${\theta^{**}}_{max}$. Thus one has 400 by 400 points of (Q^{**}, θ^{**}) which uniquely correspond to (Q, θ). Within each cell, a bi-linear interpolation is used to calculate (U, θ) which is not on the grid point. The true instantaneous velocity components are calculated from $U = Q\cos\theta, \quad V = Q\sin\theta$.

Before the actual measurements were taken, the detailed accuracy and resolution analysis were made. It was noticed that with the transformation described by Panchepakesan and Lumley (1993) the yaw angle resolution at low velocities was significantly improved.

To determine all the flow fluctuations to a reasonable accuracy, it is important that a reliable detection scheme be used. The oscillation frequency of the jet was found in the range of 10 - 100HZ. The jet oscillation frequency was easily controlled by the nozzle upstream pressure, width of the nozzle throat, the length and the diameter of the communicating loop as shown in figure (3). Data was taken at the rate of 10KHz for 5 seconds. The hot wire measurement cut off frequency was 4KHz. Local averaging was used to determine the threshhold levels to each period of the flow. A typical number of realizations

for the ensemble averaging was 100.

Experimental Results and Discussion

Calibration

Figures 7(a)-(c) show the calibration domain and the velocity surface grid in the original variables; while figures 8(a)-(c) present the results in the transformed intermediate variables. This type of full-velocity yaw angle look-up table calibration method has many advantages over variable angle methods or other conventional approaches. For example, no calculation of partial derivatives are needed; no physical laws governing the hot wire are needed. Also one can see, from figures 7 and 8, that while the conventional method uses only 1/3 of the domain, the transformed method employs most of calibration domain. This means higher efficiency and resolution can be achieved. The uncertainty of the crossed hot wire measurements was found to be less than 1% (Panchapakesan and Lumley, 1993), while the calibration without this transformation has the accuracy of 2.5%. Detailed resolution and uncertainty analysis can be found in Herr (1994).

Detection of deterministic flow structure

Throughout this study the results from a fixed jet oscillation frequency of 80 Hz is presented. However, the results from other frequencies in a range from 10 to 100 Hz are discussed in Herr (1994). Figure 9 shows the process of detecting the deterministic flow structure by ensemble averaging technique. Figure 9(a) is the instantaneous velocity measured by crossed wire. It can be roughly seen that the flow is periodic and that the turbulence is on top of the deterministic part of the flow. Figures 9(b) and 9(c) are ensemble averaged data with 40 and 70 realizations, respectively. It can be observed that 40 realization averaging does not eliminate the turbulence influence while 70 realization averaging is better smoothed but small non-deterministic fluctuations are still visible. Figure 9(d) is the ensemble averaged measured data with 100 realizations and its comparison with corrected similarity solution discussed in the previous paragraphs. The ensemble averaged measured deterministic velocity is smooth and matches the similarity solution well. Figure 9(d) shows that corrected similarity solution predicts instantaneous deterministic velocity with reasonable accuracy.

Oscillatory stress measurements and comparison with the corrected similarity solution

Figure 10 is the time averaged and ensemble averaged turbulence stress. It can be seen that the itme averaged turbulent stress and ensemble averaged turbulent stress values are very close to each other. Curve fitting of ensemble averaged data was used in numerical iteration process described in the previous paragraphs. Figures 5(a) and 5(b) present the instantaneous deterministic velocity predictions at $x/d = 60$, where η takes an approximate value of 0.35 at the edges of the jet. The figure gives wave form of two complete cycles. In figure 5(a) axial component has two peaks within each cycle when $\eta \leq 0.003$. For the range of $0.003 \leq \eta \leq 0.350$ only one peak for each cycle can be detected. This is because of the fact that in the center region the jet passes the location twice in each period and in outer region the jet sweeps only once. Figure 5(a) also gives an hint on the intensity of the oscillation. The oscillation amplitude is smallest at $\eta = 0$ and gradually increases to its maximum at $\eta = 0.1 \sim 0.2$, and then it decreases to zero at jet edges. Figure 5(b) indicates the lateral instantaneous deterministic velocity components. Different from axial component, the lateral component has only one peak in each cycle in the entire region.

Figure 6 shows a series of axial deterministic velocity predictions as function of time during a complete period. One can clearly see that the high kinetic energy region oscillates in the flow field and that this region sweeps a much wider domain than the steady jet.

Mean velocity

The predicted and measured axial mean velocity distributions as a function of η are shown in figure 11 and lateral mean velocity profile in figure 12. From this point on, the thick solid lines indicate corrected similarity predictions and all other relatively thinner lines show curve fits to the measured data. In this figure, U_m, the scale velocity, is the centerline mean velocity. The axial mean velocity profile of the oscillatory flow is fuller than that of steady flow. This is expected because oscillation increases spreading rate as observed by many other authors. Figure 12 also shows that oscillation causes larger lateral mean velocity in the core of the jet where $\eta < 0.14$ for $x/d = 60$ which dictates enhanced transport in lateral direction.

Figures 11 and 12 compare the corrected oscillation similarity solution with measured data for both steady and oscillatory cases. From figure 11 one can see that

the corrected similarity prediction is very close to the measurements when $0 \leq \eta \leq 0.275$. Figure 12 shows that the lateral prediction compares well with measured hot wire data is when $0 \leq \eta \leq 0.20$.

Shear stresses

Figures 13 and 14 show the shear stress distributions for steady and oscillatory flows at $x/d = 60$. All of the measured profiles show that shear stresses are zero at the centerline and have peaks at location between the edge and the centerline. Both turbulence and oscillation stresses for unsteady flow are smaller than those in steady flows. But the sum of them is relatively higher compared to that of the steady jet.

In addition to turbulent shear stresses $< uv >$ and oscillation stresses $< u^*v^* >$, the correlations between oscillation and turbulence are also provided in figures 13 and 14. In both figures, it is clear that $< u^*v >$ and $< uv^* >$ are several order of magnitude lower than the oscillation and turbulence stresses. Quantitatively, both $< u^*v >$ and $< uv^* >$ are less than 1 % of $< uv >$ and $< u^*v^* >$. Figures 13 and 14 clearly shown the neglegible quantities $< u^*v >$ and $< uv^* >$. These data experimentally verified the theory proposed and proved as shown in Herr and Camci (1994).

Oscillation stress predictions by the current model and comparison of prediction and measurements are given in figure 15. One can see that the model predicts the oscillation stress very well when $0 \leq \eta \leq 0.2$.

Kinetic energy transport

Turbulent kinetic energy $< q^2 >$ and oscillation kinetic energy $< q^{*2} >$ distributions for both steady and oscillatory jets are shown in figure 16. The sum of the turbulent kinetic energy and oscillatory kinetic energy near the jet centerline where $\eta \leq 0.05$, $x/d = 60$ is about the same as the kinetic energy of the steady jet. The total kinetic energy is greater than that of the steady jet at all points where $\eta \geq 0.05$. The normal stresses $< u^2 >$, $< u^{*2} >$ and $< v^2 >$, $< v^{*2} >$ are shown in figures 17 and 18. The distribution of the oscillatory normal stress $< v^{*2} >$ is about twice as high as the turbulent normal stress $< v^2 >$ in the region where $\eta \leq 0.1$. The two quantities merge into each other at $\eta \geq 0.15$. The $< v^2 >$ component in oscillatory flow is about the same as that of steady turbulence at the centerline. Although the steady jet $< v^2 >$ decreases monotonically after $\eta \geq 0.05$, while $< v^2 >$ for the oscillatory jet continues to increase up to $\eta = 0.14$.

Figures 17 and 18 show the strong spreading character of the deterministic oscillations clearly. A much larger area is disturbed via oscillations when compared to the steady jet. It is shown in figure 16 that most of the kinetic energy in the oscillatory jet is contained in the deterministic part.

Figures 16, 17 and 18 also show that the suggested corrected oscillation similarity solution predict the experimental data fairly accurately. The model predicts the kinetic energy distribution well when $\eta \geq 0.05$, while it slightly under predicts the kinetic energy at the centerline.

Conclusions

The unsteady oscillatory jet can be modeled by a corrected similarity solution presented in this paper. The planar self-oscillatory jet with prescribed frequency can be used in isolating the contributions of the deterministic oscillations and turbulent fluctuations on the momentum and (eventually) heat transfer process. From the previous discussions of analytical efforts and experimental observations in an oscillatory planar jet, the following conclusions are drawn.

1. The modified version of the present crossed hot wire technique improves resolution and therefore accuracy in the low speed range which is important the current study. The accuracy can be improved from 2.5% to less than 1% by applying a stretching transfprmation on raw hot wire data. The measurements of oscillatory jet shows that this approach is capable of handling unsteady turbulent flow.

2. Experimental data show that the correlation terms $< u^*v >$ and $< uv^* >$ are almost zero and can be neglected in the governing equations. This neglection simplifies the transport equations greatly. The result confirms the analytical prof of this feature presented in Herr and Camci (1994).

3. At a given time t, the unsteady oscillatory flow field can be approximately described by the solution of a stationary jet flow obtained from a nozzle attached to a relative reference frame which is oscillating at a prescribed frequency.

4. The corrected similarity solution obtained in this manner predicts planar oscillatory jet well. Mean velocities are predicted very close to the measurements except at the jet edges. Oscillation kinetic energy can be predicted at places where $\eta > 0.075$.

5. Oscillation of flows enhances transport process because of the existence of additional inertia forces (oscillation stress) $< u^*v^* >$ and additional thermal fluxes (oscillation heat flux) $< v^*\theta^* >$. Most of the kinetic energy in the oscillatory jet is contained in the deterministic part. The magnitude of the unsteady kinetic energy convection due to oscillations is about typically three times of that due to turbulence.

6. Both turbulence and oscillation stresses for the specific unsteady flow are smaller than the turbulent stresses of the stationary jets. But the sum of them is relatively higher compared to that of the steady jet. The idividual terms of the kinetic enerygy conservation equations developed from the measured data show that the convection of kinetic energy in oscillatory flows is stronger than the convection due to turbulent fluctuations.

References

Binder, G. and Favre-Marinet, M., 1973, "Mixing improvement in pulsating turbulent jets," *Proceedings of ASME Symposium on Fluid Mechanics of Mixing*, Atlanta, Ga.

Crow, S. C., and Champagne, F. H., 1971, "Orderly structure in jet turbulence", *Journal of Fluid Mechanics*, Vol. 48.

Glass, D. R., 1968, "Effects of acoustic feedback on the spread and decay of supersonic jets", *AIAA Journal*, Vol. 6., No. 10.

Herr, F., 1994, "Turbulent transport in a planar jet with self-sustained deterministic oscillations and the character of impinging region heat transfer," Ph.D thesis, Department of Aerospace Engineering, The Pennsylvania State University.

Herr, F. and Camci, C., 1994,"Turbulent transport in a planar jet with self-sustained deterministic oscillations", 1994 ASME Winter Annual Meeting, International Symposium on Unsteady Flows in Aeropropulsion: Recent Advances in Experimental and Computational Methods, Chicago, IL., Nov. 6-11, 1994.

Ho, C. M., and Huang, L. S., 1982, "Subharmonics and vortex merging in mixing layers", *Journal of Fluid Mechanics*, Vol. 119.

Hussain, A. K. M. F. , and Hasan, M. A. Z., 1983,"The 'whistler-nozzle' phenomenon", *Journal of Fluid Mechanics*, Vol. 134.

Hussain, A. K. M. F., and Reynolds, W. C., 1970. "The mechanics of an organized wave in turbulent shear flow", *Journal of Fluid Mechanics*, Vol. 41.

Lueptow. R. M., Breuer, W. K., and Haritonidis, J. H., 1988, "Computer-aided calibration of x-probes using a look-up table", *Experiments in Fluids*, Vol. 6.

Panchapakesan, N. R., and Lumley, J. L., 1993, "Turbulence measurements in axisymmetric jets of air and helium, part 1. air jet," *Journal of Fluid Mechanics*, Vol. 246.

Raman, G., Hailye, M., and Rice, E., 1993, "Flip-flop jet nozzle extended to supersonic flows", *AIAA Journal*, Vol. 28.

Rockwell, D. O., 1972, "External excitation of planar jets", *Journal of Applied Mechanics*, Vol. 39.

Schlichting, H., 1979, "Boundary-Layer Theory", McGraw-Hill Book Company.

Simmons, J. M., Lai, C. S., and Platzer, M. F., 1981, "Jet excitation by an oscillating vane," *AIAA Journal*, Vol. 19.

Simmons, J. M., Platzer, M. F., and Smith, T. C., 1978, "Velocity measurements in an oscillating plane jet issuing into a moving airstream," *Journal of Fluid Mechanics*, Vol. 84.

Strykowski, P. J., 1992, "Self-excitation and mixing in axisymmetric jets with counterflow", AIAA paper 92-0538.

Tennekes, H., and Lumley, J. L., 1972, " A first course in turbulence", MIT Press.

Viets, H., 1975, " Flip-flop jet nozzle," *AIAA Journal*, Vol. 13.

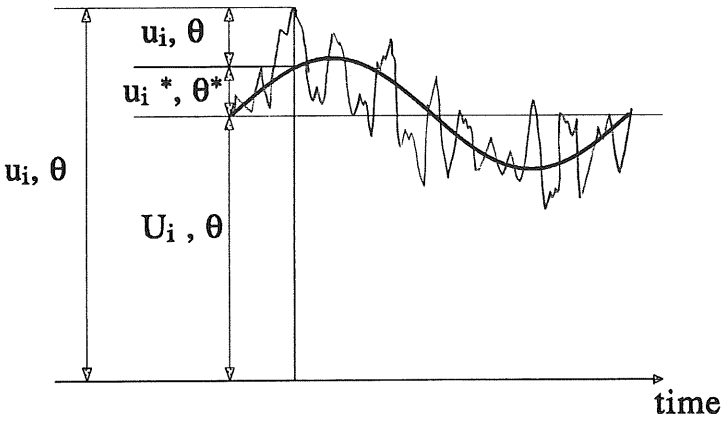

Figure 1: Decomposition of instantaneous quantities.

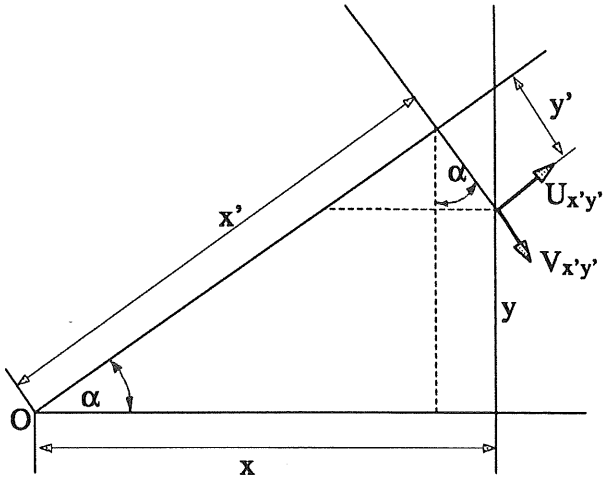

Figure 4: Sketch of corrected similarity solution. Velocity vectors as observed in the relative frame.

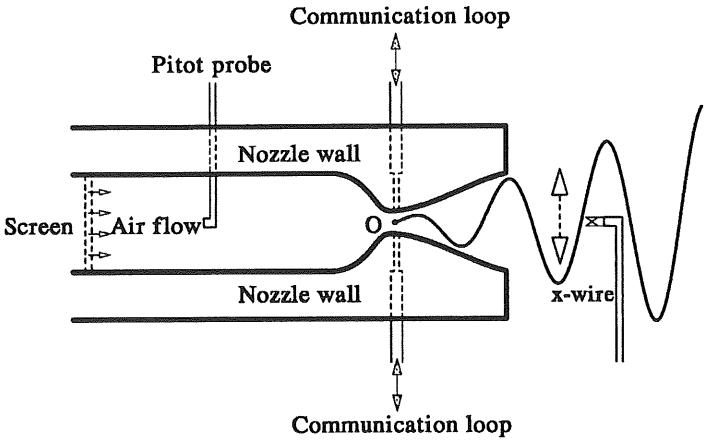

Figure 2: Nozzle configuration.

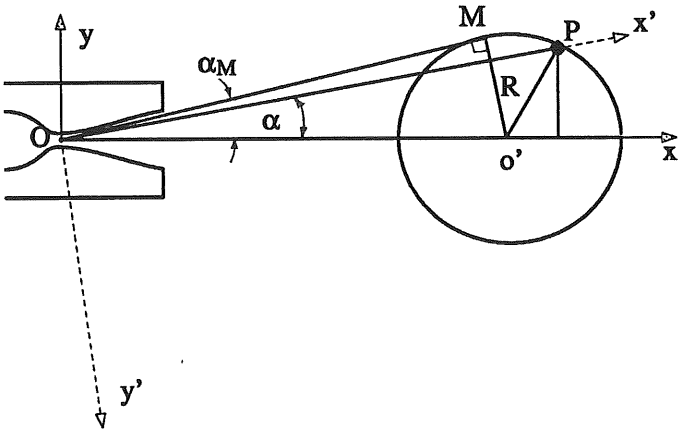

Figure 3: Nozzle oscillation modelling. α as a function of time t.

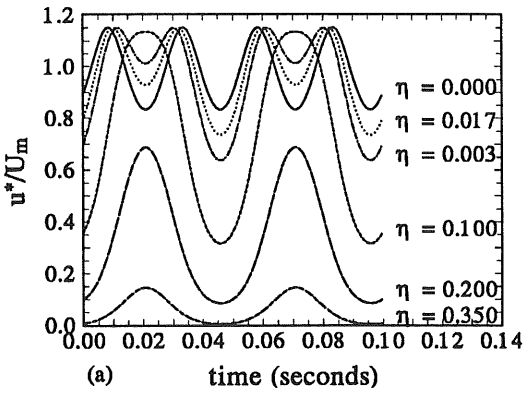

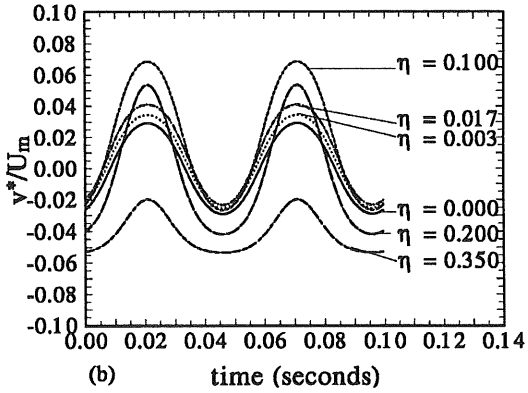

Figure 5: Instantaneous deterministic velocity predictions using the corrected similarity model, where $u^* = U^* - U$, $v^* = V^* - V$. The calculations were taken at $x/d = 60$, $f = 80Hz$, $\eta = 0.20$.

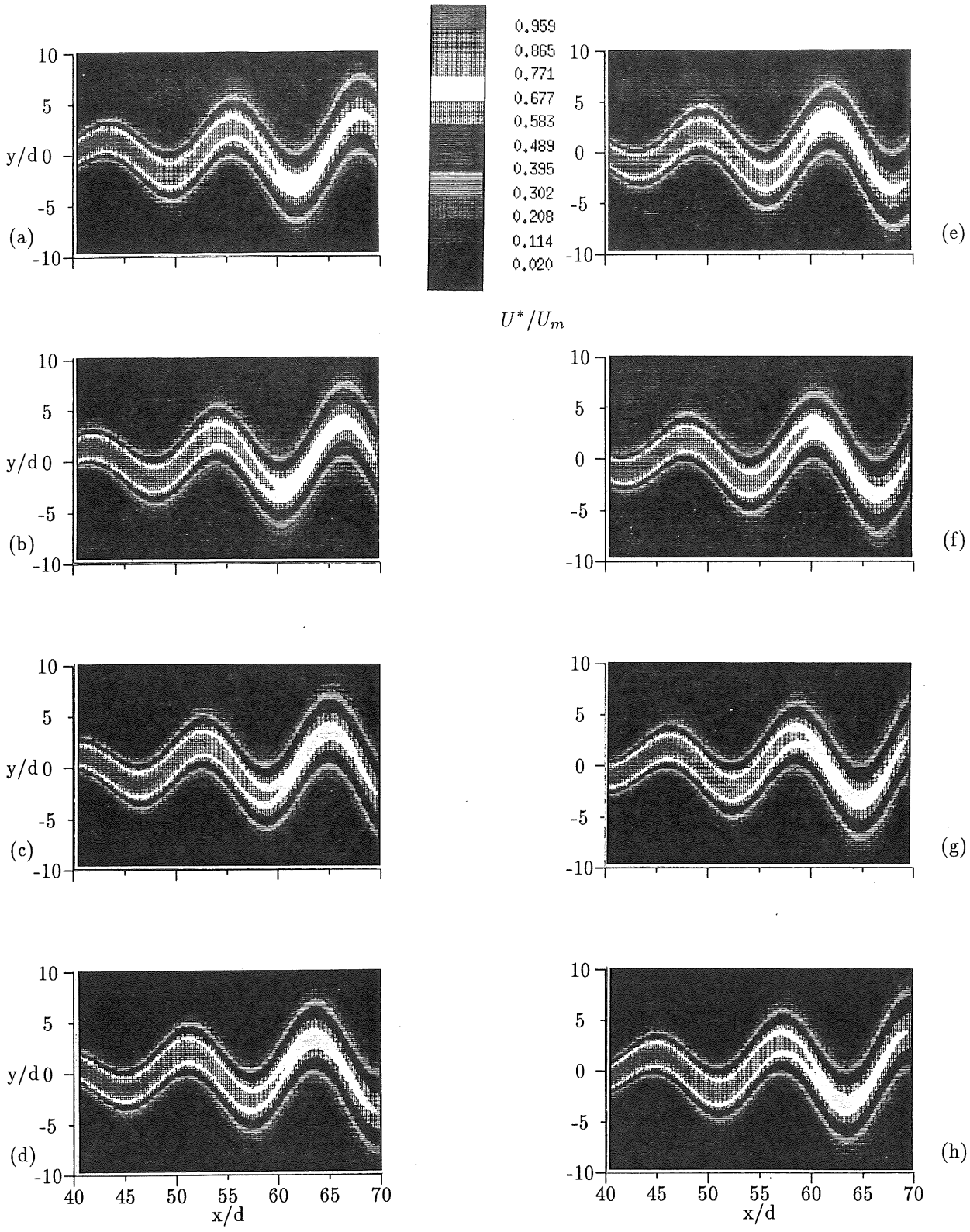

Figure 6: Instantaneous deterministic unsteady velocity contours (U^*/U_m).
(a) $t = \frac{0}{8}T$. (b) $t = \frac{1}{8}T$. (c) $t = \frac{2}{8}T$. (d) $t = \frac{3}{8}T$. (e) $t = \frac{4}{8}T$. (f) $t = \frac{5}{8}T$.
(g) $t = \frac{6}{8}T$. (h) $t = \frac{7}{8}T$.

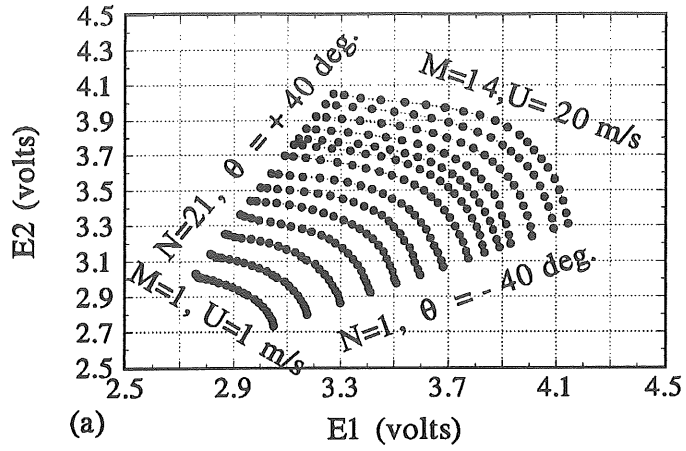

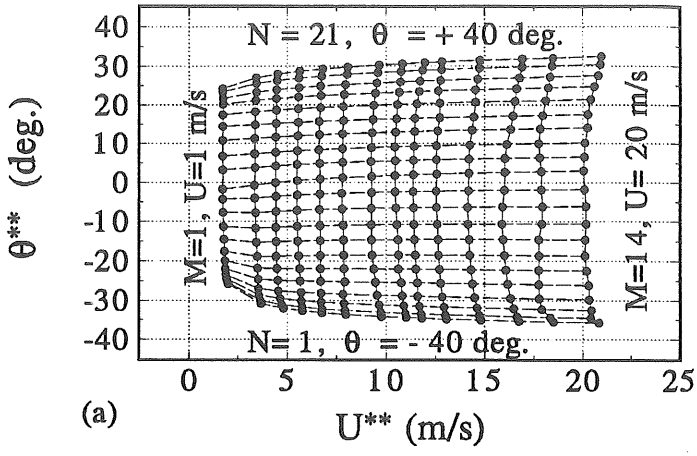

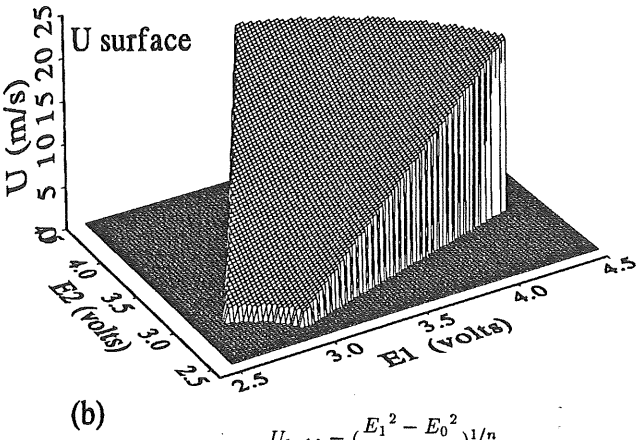

$$U_{1eff} = \left(\frac{E_1^2 - E_0^2}{A}\right)^{1/n}$$

$$U_{2eff} = \left(\frac{E_2^2 - E_0^2}{A}\right)^{1/n}$$

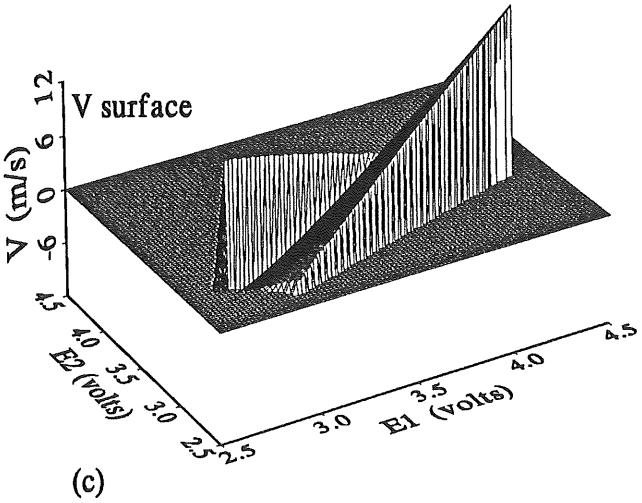

Figure 7: Crossed hot wire calibration scheme without transformation. (a) Calibration domain in the original variables. (b) U velocity surface. (c) V velocity surface.

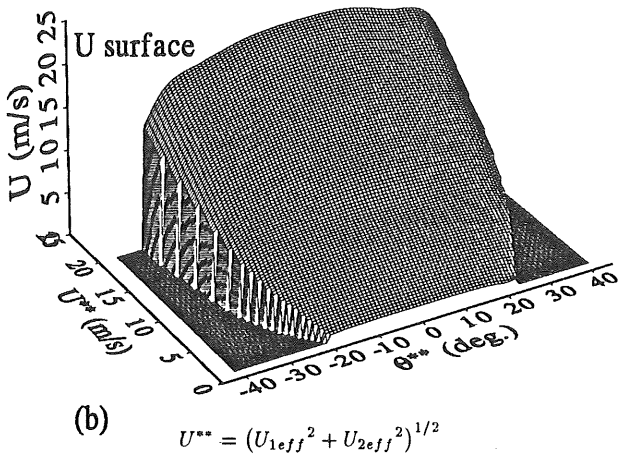

$$U^{**} = \left(U_{1eff}^2 + U_{2eff}^2\right)^{1/2}$$

$$\theta^{**} = \tan^{-1}\left(\frac{U_{2eff}}{U_{1eff}}\right) - \frac{\pi}{4}$$

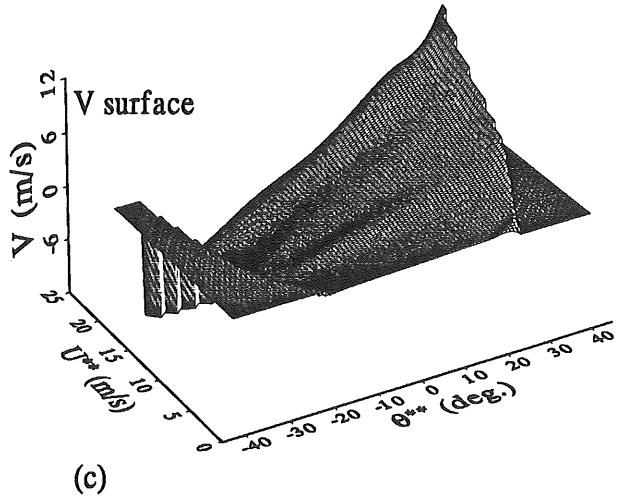

Figure 8: Crossed hot wire calibration scheme with transformation. (a) Calibration domain in the intermediate variables. (b) U velocity surface. (c) V velocity surface.

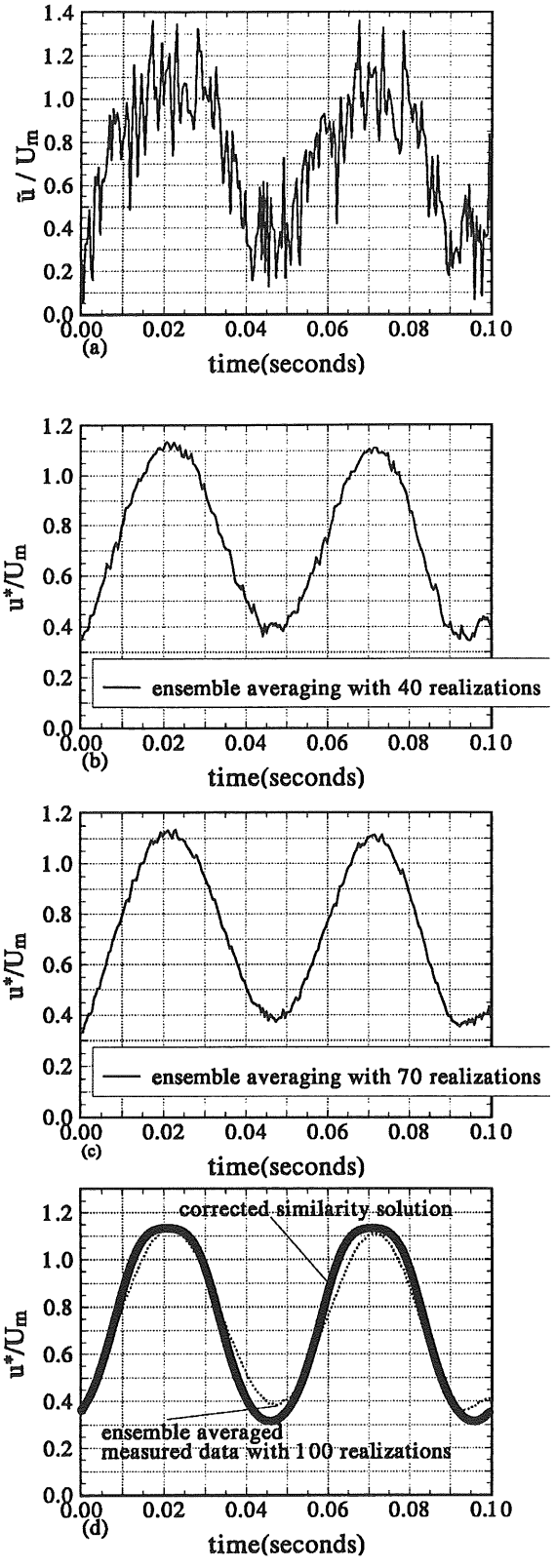

Figure 9: Ensemble averaging scheme and its comparison with corrected similarity solution. (a) Instantaneous velocity. (b) Ensemble averaged measured data with 40 realizations. (c) with 70 realizations. (d) with 100 realizations and comparison with prediction, $x/d = 60$, $f = 80Hz$.

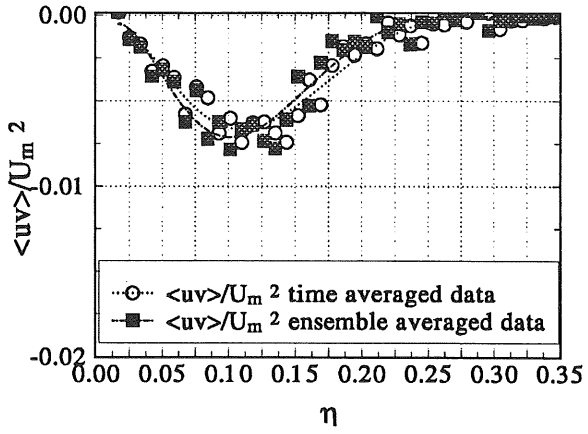

Figure 10: Time averaged and ensemble averaged Reynolds stresses, $x/d = 60$, $f = 80Hz$.

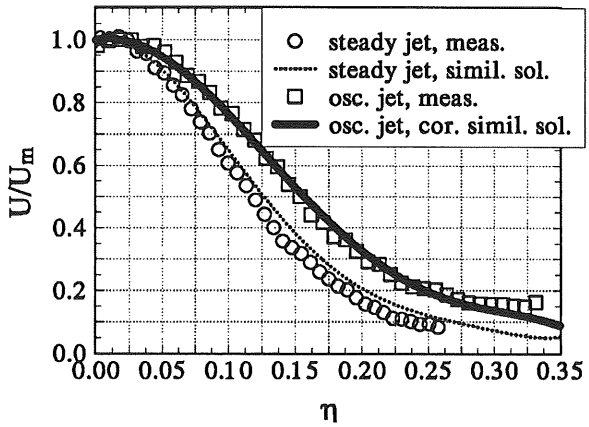

Figure 11: Axial mean velocity profiles across the jet, $x/d = 60$, $f = 80Hz$.

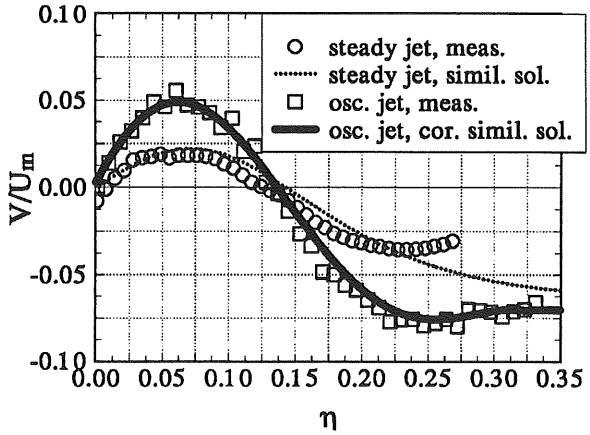

Figure 12: Lateral mean velocity profiles across the jet, $x/d = 60$, $f = 80Hz$.

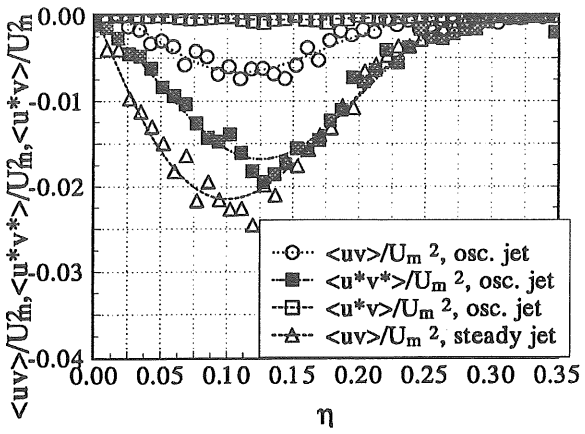

Figure 13: Turbulence, oscillation stresses and correlation between u^* and v, $x/d = 60$, $f = 80Hz$.

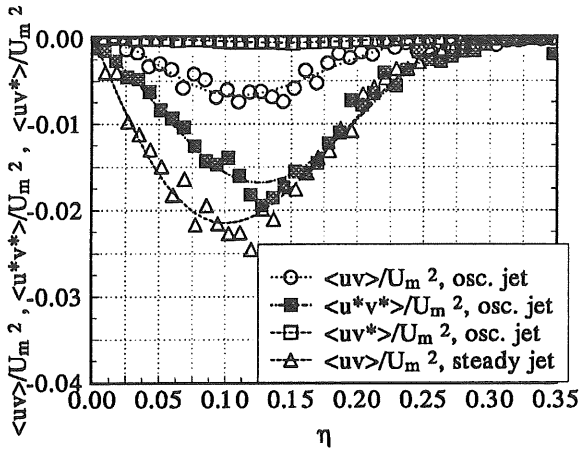

Figure 14: Turbulent, oscillation stresses and correlation between u and v^*, $x/d = 60$, $f = 80Hz$.

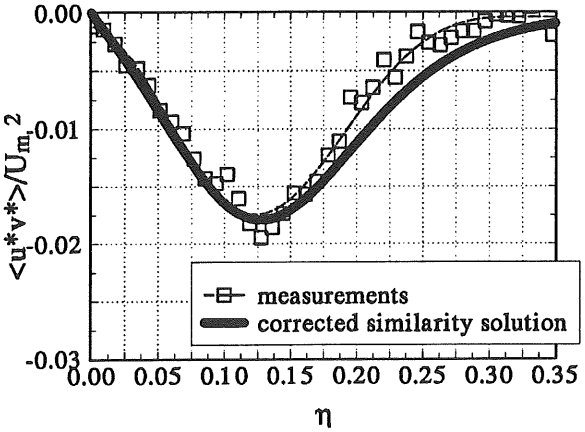

Figure 15: Oscillation shear stress and comparison with the corrected similarity solution, $x/d = 60$, $f = 80Hz$.

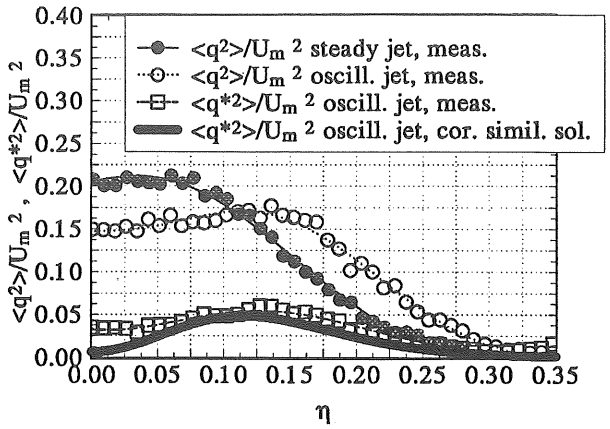

Figure 16: The measured kinetic energy and comparison with the corrected similarity solution, $x/d = 60$, $f = 80Hz$.

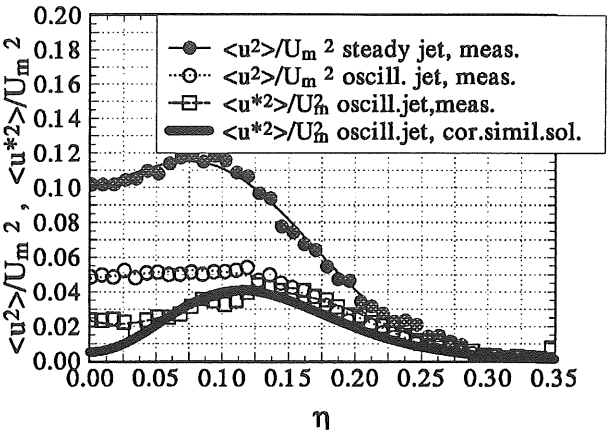

Figure 17: The measured normal stress components and comparisons with the corrected similarity solution. Axial component (u^2), $x/d = 60$, $f = 80Hz$.

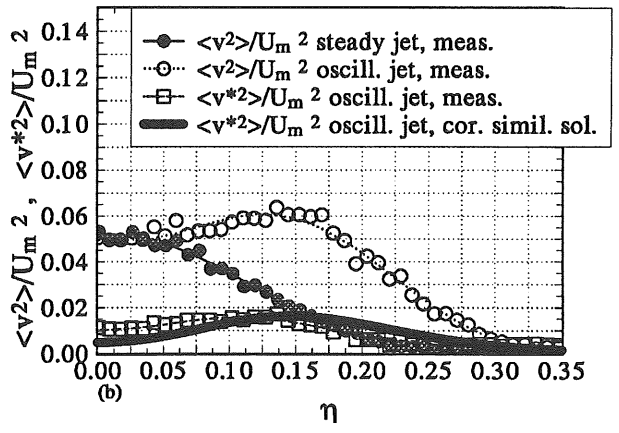

Figure 18: The measured normal components and comparisons with the corrected similarity solution. Lateral component (v^2), $x/d = 60$, $f = 80Hz$.